

Muon spin spectroscopy in multiferroic $(\text{Cu,Zn})_3\text{Mo}_2\text{O}_9$

Haruhiko KUROE¹, Kento AOKI¹, Tasuku SATO¹, Ryo KINO¹, Hideki KUWAHARA¹, Tomoyuki SEKINE¹, Masashi HASE², Ikuto KAWASAKI³, Takayuki KAWAMATA^{3,4}, Takao SUZUKI^{3,5}, Isao WATANABE³, Kunihiko OKA⁶, Toshimitsu Ito⁶, and Hiroshi EISAKI⁶

¹ *Physics Division, Sophia University, 7-1 Kioi-cho, Chiyoda-ku, Tokyo 102-8554, Japan*

² *National Institute for Materials Science (NIMS), Tsukuba, Ibaraki 305-0047, Japan*

³ *Advanced Meson Science Laboratory, RIKEN Nishina Center, Wako, Saitama 351-0198, Japan*

⁴ *Department of Applied Physics, Graduate School of Engineering, Tohoku University, Aoba-ku, Sendai 980-8579, Japan*

⁵ *College of Engineering, Shibaura Institute of Technology, Minuma, Saitama 337-8570, Japan*

⁶ *National Institute of Advanced Industrial Science and Technology (AIST), Tsukuba, Ibaraki 305-8568, Japan*

E-mail: kuroe@sophia.ac.jp

(Received October 1, 2018)

We present the muon spin relaxation/rotation spectra in the multiferroic compound $(\text{Cu,Zn})_3\text{Mo}_2\text{O}_9$. The parent material $\text{Cu}_3\text{Mo}_2\text{O}_9$ has a multiferroic phase below $T_N = 8.0$ K, where the canted antiferromagnetism and the ferroelectricity coexist. The asymmetry time spectra taken at RIKEN-RAL pulsed muon facility show a drastic change at T_N . At low temperatures the weakly beating oscillation caused by the static internal magnetic fields in the antiferromagnetic phase was observed in $\text{Cu}_3\text{Mo}_2\text{O}_9$ and the lightly (0.5%) Zn-doped sample. From the fitting of the oscillating term, we obtain the order parameter in these samples: ferromagnetic moment in two sublattices of antiferromagnet. In the heavily (5.0%) Zn-doped sample, the muon-spin oscillation is rapidly damped. The frequency-domain spectrum of this sample suggests a formation of magnetic superstructure.

KEYWORDS: μSR , quantum spin system, multiferroic material

1. Introduction

Physics on quantum magnet has been attracted much attention. One of the most interesting effects is a quantum phase transition (QPT). It has been studied in many kinds of quantum magnets, such as an interacting antiferromagnetic (AFM) spin dimer system described well by using the bond-operator theory [1]. In this system, a pair of $S = 1/2$ spins forms a spin-singlet dimer. As a result of interaction between spin dimers, the magnetic excitation becomes dispersive. The ground state is nonmagnetic and its magnetic excitations are characterized by a spin gap much smaller than the amplitude of the AFM exchange interaction along the path forming the spin dimer. In the case when magnetic field or pressure suppresses the spin gap, the ground state becomes a mixed singlet-triplet state; the system becomes magnetic [1].

As well as external fields, impurity substitution has a potential to cause QPT from the gapfull state to a gapless AFM one. In this proceeding paper, we focus on site substituted systems. $\text{Tl}(\text{Cu,Mg})\text{Cl}_3$ system gives a good example [2–4]. QPT occurs through the following process: (i) A nonmagnetic Mg^{2+} ion is substituted for a $S = 1/2$ Cu^{2+} ion so that the singlet ground state of spin dimers is broken; (ii) As a result, a nonmagnetic impurity substitution induces unpaired spins with $S = 1/2$; (iii) Impurity-induced AFM state is formed through the interaction between the unpaired spins. This process is known as an ‘order by disorder’ effect. The muon spin spectroscopy has been applied to this system as an efficient local probe [5–9].

In this study, we focus on QPT in $(\text{Cu,Zn})_3\text{Mo}_2\text{O}_9$ induced by the site substitution. The parent material, $\text{Cu}_3\text{Mo}_2\text{O}_9$, has a multiferroic phase, where the slightly canted antiferromagnetism and the spin-driven ferroelectricity coexist [10, 11]. From the viewpoint of magnetism, this compound has a unique distorted tetrahedral spin chain made from $S = 1/2$ Cu^{2+} ions, where quantum fluctuations from the low dimensionality and geometrical spin frustration effects coexist. The magnon dispersion curve obtained by inelastic neutron scattering shows that the spin system is regarded as the AFM spin dimers indirectly interacting with each other through the quasi-one dimensional spin system [12–14]. We will show magnetization in $(\text{Cu,Zn})_3\text{Mo}_2\text{O}_9$ system in the following section. The multiferroic properties in the Zn-5.0% sample, including temperature and magnetic-field dependences of (differential) magnetization, dielectric constant, a electric-polarization-electric-field loop, and specific heat have been reported in our recent publication [15]. In this proceedings paper, we focus on the muon-spin relaxation/rotation (μSR) spectra in $(\text{Cu,Zn})_3\text{Mo}_2\text{O}_9$ at zero magnetic field.

2. Experiments

2.1 Samples

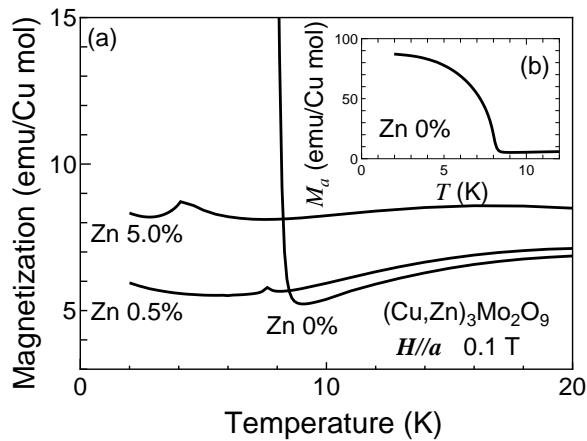


Fig. 1. (a) Temperature variations of magnetization at 0.1 T in $(\text{Cu,Zn})_3\text{Mo}_2\text{O}_9$ with Zn concentrations of 0%, 0.5%, and 5.0%. (b) Reduction of the low-temperature magnetization in $\text{Cu}_3\text{Mo}_2\text{O}_9$.

The single crystals of $(\text{Cu,Zn})_3\text{Mo}_2\text{O}_9$ were prepared with the continuous solid-state crystallization method by using an infrared furnace utilized for the floating-zone method [16]. This method gave single crystals of highly homogeneous impurity substitution because they were grown *without* melting. We prepared platelike single crystals of $\text{Cu}_3\text{Mo}_2\text{O}_9$ and the Zn-0.5% and the Zn-5.0% substituted samples by slicing them perpendicular to the a axis. The thickness of the sample is chosen to be 350 μm , which is enough to stop the muon beam.

To explain the magnetic properties in these samples, we show their magnetizations as functions of temperature in Fig. 1. As shown in Fig. 1(b), a sharp increase of the magnetization M_a along the a axis with decreasing temperature below T_N was observed in $\text{Cu}_3\text{Mo}_2\text{O}_9$. As will be discussed later in detail, this increment is due to the weak ferromagnetic moment in the canted AFM phase induced by magnetic fields. In the Zn-0.5% and the Zn-5.0% samples, as shown in Fig. 1(a), small cusps were observed instead of the increase of magnetization due the spin canting. Moreover, a small increase of magnetization probably obeying a Curie-Weiss law was observed at low temperatures. The origin of it is thought to be the disorder effects on the distorted tetrahedral spin chains which include the unpaired spins on the AFM spin dimers induced by the nonmagnetic Zn doping.

2.2 μ SR measurements

The μ SR time spectra are measured using the pulsed surface muon at RIKEN-RAL muon facility, of which momentum and kinetic energy are 29.79 MeV/c and 4.119 MeV, respectively [17]. The single crystals were mounted on the high-purity silver plate using Apiezon N grease, so that the muon beam with a diameter of $\phi 25$ mm is irradiated efficiently. The spin polarization of implanted muons is parallel to the a axis, along which the spontaneous magnetization is observed. This is not the direction of spin chain; the weak ferromagnetic components of the spin moments of the distorted tetrahedral spin chains at the center and the corner of the orthorhombic unit cell direct to the direction of $\pm 23.2^\circ$ from the a axis, respectively [10]. They have both of the weak ferromagnetic components along the a and c axes, the latter of which are canceled in the unit cell. The single crystals were cooled down to 0.3 K in a ^3He cryostat with a charcoal sorption pump. To ensure thermal contact, the samples were wrapped tightly in a silver foil (thickness 25 μm). The observed μ SR asymmetry parameter $A_{\text{obs}}(t)$ was defined as

$$A_{\text{obs}}(t) = \frac{F(t) - \alpha B(t)}{F(t) + \alpha B(t)}, \quad (1)$$

where $F(t)$ and $B(t)$ were the total muon events counted by the forward and the backward counters at time t , respectively. The factor α calibrates relative counting efficiencies between them. The α is obtained from the $A_{\text{obs}}(t)$ above T_N under a weak transverse magnetic field, which is a standard method to calibrate α . Raw data of $A_{\text{obs}}(t)$ contain the signals from muons stopped at the Ag foil and the sample holder, A_{Ag} , of which value (about 6%) depends on the measurement setting. These unwanted components were removed by using $A_{\text{obs}}(t)$ measured under the weak transverse magnetic field at temperatures much below T_N , which is also a standard method to obtain A_{Ag} . We introduce a corrected asymmetry spectrum $A(t)$ at temperature T as $[A_{\text{obs}}(t) - A_{\text{Ag}}]$ normalized by $[A_{\text{obs}}(0) - A_{\text{Ag}}]$ at 10 K, so that $A(t)$ at 10 K decays from $A(0) = 1$. Here 10 K is chosen as a temperature well above T_N .

3. Results

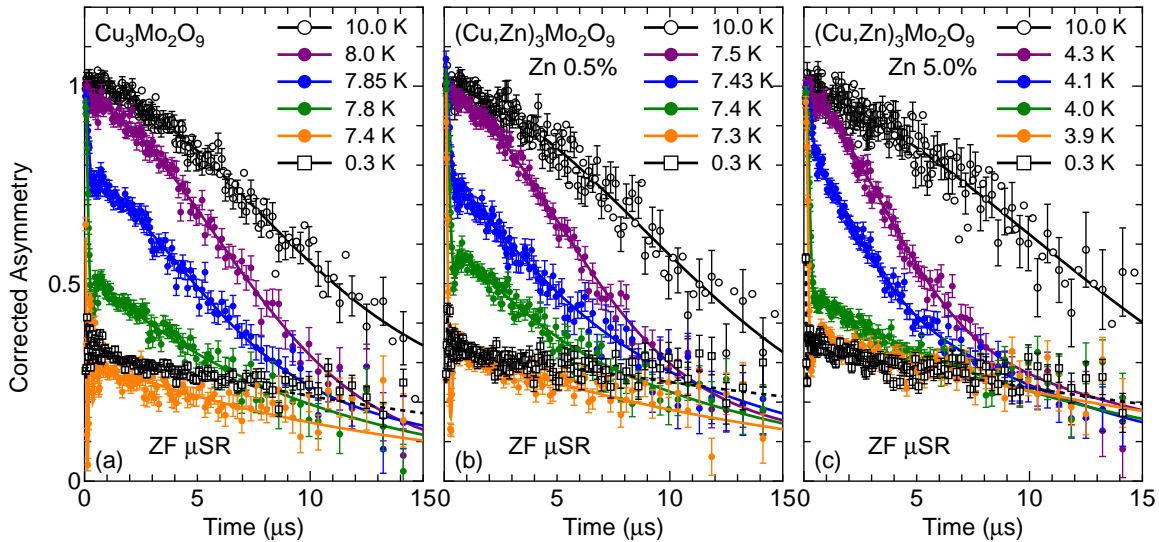


Fig. 2. (color online) Muon time spectra in $\text{Cu}_3\text{Mo}_2\text{O}_9$ at various temperatures below and above T_N and those in the samples with Zn-0.5% and Zn-5.0% substitutions shown in (a), (b), and (c), respectively.

Figures 2(a)-2(c) show $A(t)$ in $\text{Cu}_3\text{Mo}_2\text{O}_9$ and the Zn-0.5% and the Zn-5.0% substituted samples, respectively. At 10 K, well above T_N , $A(t)$ seems to obey a Gaussian function. We call this component the G term. The G term appears as a small- t part of the Kubo-Toyabe relaxation function which reproduces the muon spin relaxation of the paramagnetic polycrystal where randomly aligned static internal fields work at the muon sites. Here the word ‘static’ indicates that the time scale of internal field fluctuation is much slower than the time scale of μSR measurement ($10^{-6} - 10^{-5}$ sec). Reflecting critical phenomena, the G term rapidly disappears with decreasing temperature just below T_N .

At 0.3 K, well below T_N , $A(t)$ seems to show an exponential decay from $A(0)$ much smaller than the unity. We call this term the Lorentzian term or the L term, in a customary way of muon spectroscopy. The L term is observed through the strong collision model with the dynamical fluctuation of internal fields of which time scale is much faster than the time scale of μSR measurement. The L term was observed even above T_N as a background of the Gaussian term. $A(0)$ below T_N is much smaller than the unity, suggesting that there is a rapid damping term of which damping speed is much faster than the dead time of μSR measurement. Because this component is undetectable with a pulsed muon source, we call this term ‘missing term’ or the M term.

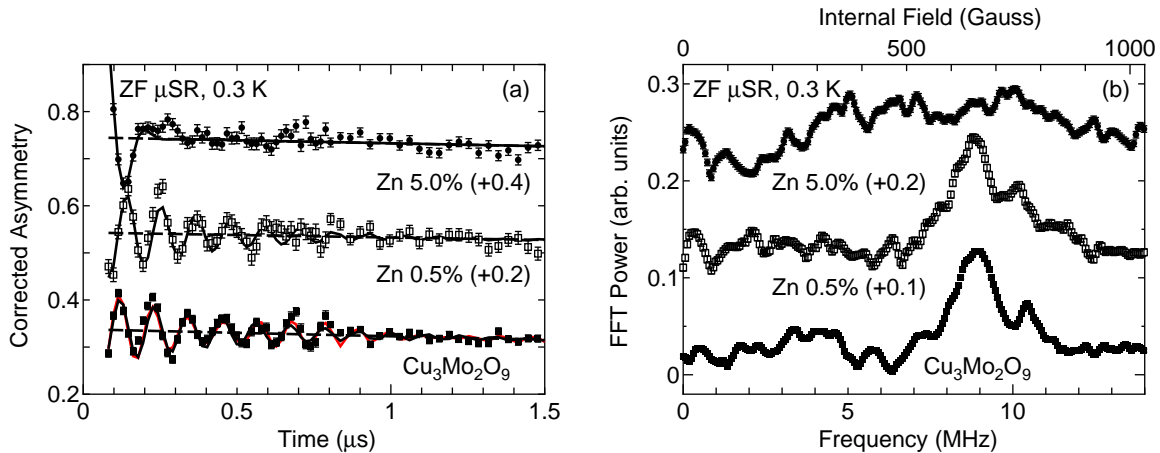


Fig. 3. (color online) (a) Muon time spectra at 0.3 K in $\text{Cu}_3\text{Mo}_2\text{O}_9$ and those in the samples with Zn-0.5% and Zn-5.0% substitutions. The oscillating and exponentially decaying components are shown by the solid and the dashed curves, respectively. The red curve denotes the oscillating component obtained by using the two oscillator model, of which the details are given in the text. (b) The fast Fourier transformation power spectra of oscillating terms.

As expanded in Fig. 3(a), $A(t)$ contains an oscillating term. We call it the O term. The oscillation of $A(t)$ of $\text{Cu}_3\text{Mo}_2\text{O}_9$ in Fig. 3(a) shows beat signals around 0.25 and 0.75 μs . It was clearly shown in its fast Fourier transformation in Fig. 3(b) as a two-peak structure with the internal fields of 667 and 760 Gauss. The oscillating component and its fast Fourier transformation of the Zn-0.5% substituted sample is qualitatively similar to those of $\text{Cu}_3\text{Mo}_2\text{O}_9$. The fast Fourier transformation of this sample seems to have a main component at 667 Gauss. However, the noisy spectrum prevented us from obtaining the detailed structure above 700 Gauss. This is due to the noisy spectrum around $t \sim 0.7$ μs while the beat signals were clearly observed around 0.7 μs in case of $\text{Cu}_3\text{Mo}_2\text{O}_9$. The possible origins of the beating oscillation in time-domain spectra and the multipeak structure in frequency-domain spectra are thought to be the phase separation and/or the multiple muon stopping sites. The $A(t)$ and its fast Fourier transformation in the Zn-5% sample are very different from those in other samples. The damping rate of oscillation in $A(t)$ is much faster. The internal field has a very broad spectrum around 500 Gauss. These indicate widely distributed internal fields.

Next, let us discuss the fitting function. Unfortunately, there is no function which fits all the data in all the samples. And then, we need to combine two components each of which has the Gaussian or the Lorentzian decay. The fitting function of $A(t)$ above T_N in all the samples is

$$A_{\text{HT}}(t) = A_G \exp[-(\sigma_G t)^2] + A_L \exp[-\lambda_L t], \quad (2)$$

where the suffix G(L) denotes the quantity for the Gaussian (Lorentzian) decay with a specific rate σ_G (λ_L). Here we introduced the condition of $A_G + A_L = 1$ for amplitude parameters A_G and A_L .

Below T_N , we consider the main component of the O term in cases of $\text{Cu}_3\text{Mo}_2\text{O}_9$ and the Zn-0.5% sample, which oscillates with the frequency γH_{int} , where γ and H_{int} are the gyromagnetic ratio of muon and the internal field at the muon stopping site(s), respectively, which leads the strongest amplitude in fast Fourier transformations. Reflecting the frequency domain spectrum in Fig. 3(b), the damping factor of the oscillating term is chosen to be the exponentially decaying function and $A(t)$ is given as:

$$A_{\text{LT-L}}(t) = A_O \cos[\gamma H_{\text{int}} t + \phi] \exp[-\lambda_O t] + A_L \exp[-\lambda_L t], \quad (3)$$

with the factor $A_M \equiv 1 - A_O - A_L$ which corresponds to the decrease of the initial asymmetry at 0.3 K; in other words, it corresponds to the amplitude of the M term. Here the phase factor ϕ is introduced phenomenologically. One can see that this model could not reproduce the beat of the μSR time spectra in Fig. 3(a) because the dominating oscillator with a single frequency is considered. For comparison, we introduce the two oscillators model where the term of $A'_O \cos[\gamma H'_{\text{int}} t + \phi] \exp[-\lambda'_O t]$ is added to eq. (3). We show the fitting result by the red curve in Fig. 3(a). The beating spectrum is reproduced slightly better when we fit it to the two oscillators model; however, the obtained parameters of the dominating oscillator are not changed within the experimental accuracy as listed in the following table:

Model	Corrected Initial Asymmetry (%)	A_O or A'_O (%)	H_{int} or H'_{int} (Gauss)	λ_O or λ'_O (MHz)
One Oscillator Model	42.53±0.65	8.73±0.65	667.0±1.5	2.31±0.22
Two Oscillators Model	43.82±0.55	8.54±0.53	665.8±1.4	2.14±0.19
		1.49±0.19	759.1±1.6	0.61±0.22

Table I. Corrected initial asymmetries, the relative amplitudes, the internal fields, and the damping factors obtained by using the one oscillator and the two oscillators models.

Hereafter, we fit the experimental data to the one oscillator model which leads the precise parameters within experimental error. This model is applicable to the μSR time spectra at high temperatures and those in the Zn-substituted samples, which are slightly scattered due to short accumulation times.

For $A(t)$ below T_N in the Zn-5.0% sample, the widely distributing internal fields in the O term are reproduced by a Gaussian distribution, as shown in Fig. 3(b). And then, the fitting function becomes

$$A_{\text{LT-G}}(t) = A_O \cos[\gamma H_{\text{int}} t + \phi] \exp[-(\sigma_O t)^2] + A_L \exp[-\lambda_L t], \quad (4)$$

with the factor $A_M \equiv 1 - A_O - A_L$. The relative amplitude-temperature diagrams are given in Figs. 4(a)-4(c). Here the critical temperature is optimized so that the critical exponent of the internal field becomes 0.5. As will be mentioned later, this value is predicted by using the molecular-field theory. The T_N s in all the samples obtained from the μSR measurements are consistent with the ones obtained from magnetization.

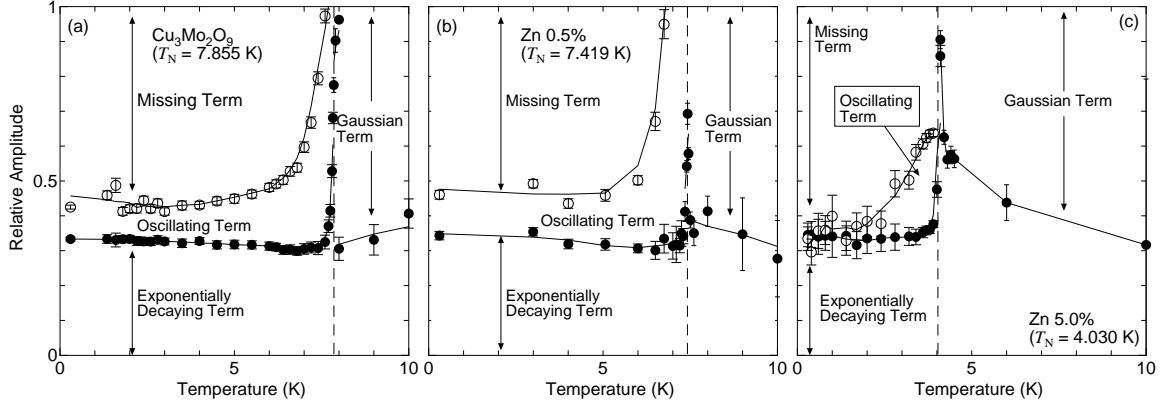


Fig. 4. Amplitudes of A_L (closed circles) below and above T_N and $A_L + A_O$ (open ones) below T_N in (a) $\text{Cu}_3\text{Mo}_2\text{O}_9$, (b) the Zn-0.5% doped sample, and (c) the Zn-5.0% doped one. The dashed lines denote T_N s. The curves denoting the relative amplitudes in these diagrams are only eye guides generated by the smoothed data.

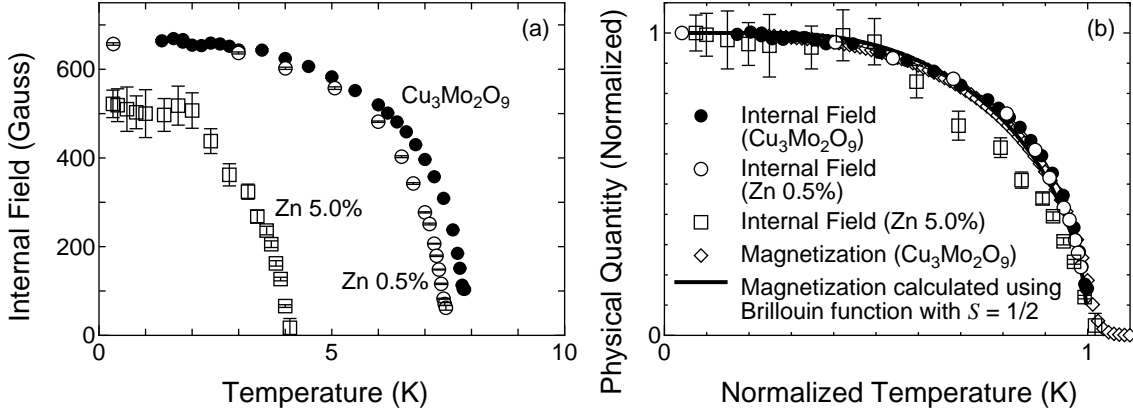


Fig. 5. (a) Internal field in $\text{Cu}_3\text{Mo}_2\text{O}_9$ (closed circles), the Zn-0.5% (open circles) sample, and the Zn-5.0% one (squares). (b) The normalized internal fields with the same symbols as in (a) and the normalized magnetization (diamonds). The magnetization calculated using the Brillouin function is shown by the bold curve. All the physical quantities are normalized by the values at the lowest temperatures.

Finally, in all the samples, we measured $A(t)$ at several temperatures and obtained H_{int} as functions of temperature. The results are given in Fig. 5(a). Because these temperature dependences are similar to one another, we normalized the abscissa by T_N and the ordinate by the values at the lowest temperature. The results are shown in Fig. 5(b).

4. Discussion

4.1 Magnetic Order Parameter

At temperatures just below T_N , A_G disappears completely and A_O increases. These are due to the formation of slightly canted AFM order. The μSR spectra in $\text{Cu}_3\text{Mo}_2\text{O}_9$ and the Zn-0.5% doped sample have almost similar temperature dependence. It is shown in the oscillating spectra [Fig. 3(a)] and the distributing internal fields [Fig. 3(b)]. As shown in Fig. 5(b), the temperature dependences of internal fields in these samples are well scaled into one line. On the other hand, the temperature dependences of the magnetization in these two systems are very different: In the Zn-0.5% doped

sample, the increase of M_a caused by the spin canting under the magnetic field is not observed. These indicate that the oscillation in μ SR spectrum reflects the ferromagnetic long-range order in each sublattice which is the order parameter of AFM order. Indeed, the temperature dependence of the internal fields in these two samples are well reproduced by the temperature dependence of the spontaneous magnetization in $S = 1/2$ *ferromagnet* calculated using the Brillouin function [18].

In case of the Zn-5.0% doped sample, as shown in Fig. 3(b), the distribution of the internal field is very broad and its structure is more complicated. As shown in Fig. 5(b), the normalized internal field in this sample is slightly different from the Brillouin function. Moreover, the amplitude-temperature diagram in Fig. 4(c) does not seem to have similar temperature dependence when we compare it to those in Figs. 4(a) and 4(b). These results strongly suggest the QPT induced by impurity doping; the system probably has a different magnetic structure. The widely distributed internal field in Fig. 3(b) suggests a formation of magnetic superlattice below T_N . To discuss further, the magnetic structure determination in the Zn-5.0% doped sample is necessary.

4.2 Origin of Missing Term

Because of finite pulse width in the pulsed μ SR measurement, high-frequency signals are smeared out when the inverted frequency and the pulse width are comparable. And then, there is a sensitivity limit in H_{int} (or in precession frequency). H_{int} in the present work (~ 650 G) almost reaches this limit. And then, the oscillating term at the low temperatures is probably underestimated. To discuss more precisely, we need to consider the frequency dependence of the sensitivity seriously or to measure μ SR spectra by using continuous muon source. Both of them are beyond the scope of this paper.

4.3 Muon Stopping Sites

Figures 4(a)-4(c) show that the relative amplitude of the L term well below T_N is slightly larger than 0.3, which is almost independent of Zn concentration. This term is a constant term coupled with the dynamical spin fluctuations. Qualitatively, in all the samples, A_L is almost independent of temperature well below T_N , has a peak around T_N , and becomes about 0.3 again well above T_N . The value of $A_L \sim 1/3$ reminds us the case of ferromagnetic polycrystal at zero magnetic field: The muon spin rotation spectrum oscillates around a constant asymmetry $A/3$ with an amplitude of $2A/3$, where A is an initial asymmetry. For another example of the value of $1/3$, as is well known, the value of Kubo-Toyabe function reaches $1/3$ without considering the dynamical decaying effects. As an analogy to the value of $1/3$ appearing in these famous cases, one might think that the value of $1/3$ in the present case suggests something special. However, the value of $1/3$ in these cases is introduced through the powder average, not in the present case. Moreover, the observed spectrum contains $A_L \sim 1/3$ even in the paramagnetic phase: A dynamically fluctuating internal field works on a third of all the muons in crystal. The possible origins of this internal field are the phase separation effect and/or the two (or more than two) muon stopping sites.

5. Conclusive Remarks

We measured μ SR spectra in $\text{Cu}_3\text{Mo}_2\text{O}_9$ and the lightly and the heavily Zn-doped samples. We found that the order parameter of the phase transition at T_N was the sublattice magnetization which was μ SR detectable. This statement was confirmed in cases of $\text{Cu}_3\text{Mo}_2\text{O}_9$ and the lightly Zn-doped sample. In the heavily Zn-doped sample, the μ SR spectrum strongly suggests a formation of magnetic superlattice, which should be confirmed by using neutron diffraction.

Finally, as a proceedings paper of USM2013, we propose an application of ultra slow muon microscope: the μ SR measurement under transverse electric field to study the cross correlation effects in multiferroic material. In conventional setting of μ SR measurements, the lateral resolution (about 30 mm in diameter) and the muon penetration depth (depending on the kinetic energy of muon beam)

cannot be controlled. And then, we could not control the relative direction between the muon's polarization direction and the electric field. With higher lateral resolution and controllable muon energy due to reacceleration, the muon beam can be led into the plate-shape single crystal from the edge side, which expands the degree of freedom of experimental configurations. And then, we can detect the magnetic order induced by an electric field more efficiently. Of course, the bending of beam axis due to the static electric field working on the charge of muon may cause a problem, which will be solved by controlling the muon energy.

Acknowledgements

This work was partly supported by a Grant-in-Aid for Scientific Research (C) (No. 22540350) of The Ministry of Education, Culture, Sports, Science, and Technology, Japan.

References

- [1] M. Matsumoto, B. Normand, T. M. Rice, and M. Sigrist: Phys. Rev. B **69** (2004) 054423.
- [2] A. Oosawa, T. Ono, and H. Tanaka: Phys. Rev. B **66** (2002) 020405.
- [3] A. Oosawa, M. Fujisawa, K. Kakurai, and H. Tanaka: Phys. Rev. B **67** (2003) 184424.
- [4] Another substitution effect, namely the random bond effect, is also an interesting subject in this field. In this kind of substituted samples, the magnetic ions are not substituted and the randomness is introduced through the spin-lattice coupling. Especially, the Bose glass phase, where the quantized magnetic excitation shows the Anderson localization, has attracted much attention [M. P. A. Fisher, P. B. Wichman, G. Grinstein, and D. S. Fisher: Phys. Rev. B **40** (1989) 546.].
- [5] T. Suzuki, F. Yamada, I. Watanabe, T. Matsuzaki, T. Goto, A. Oosawa, and H. Tanaka: J. Phys. Soc. Jpn. **78** (2009) 074705.
- [6] T. Suzuki, I. Watanabe, F. Yamada, Y. Ishii, K. Ohishi, Risdiana, T. Goto, and H. Tanaka: Phys. Rev. B **80** (2009) 064407.
- [7] T. Suzuki, I. Watanabe, F. Yamada, M. Yamada, Y. Ishii, T. Kawamata, T. Goto, and H. Tanaka: J. Phys.: Conf. Ser. **225** (2010) 012054.
- [8] T. Suzuki, I. Watanabe, F. Yamada, Y. Ishii, K. Ohishi, Risdiana, T. Goto, and H. Tanaka: J. Phys.: Conf. Ser. **200** (2010) 022061.
- [9] T. Suzuki, M. Yamada, Y. Ishii, I. Watanabe, T. Goto, H. Tanaka, and K. Kubo: Phys. Rev. B **83** (2011) 174436.
- [10] T. Hamasaki, N. Ide, H. Kuroe, T. Sekine, M. Hase, I. Tsukada, and T. Sakakibara: Phys. Rev. B **77** (2008) 134419.
- [11] H. Kuroe, T. Hosaka, S. Hachiuma, T. Sekine, M. Hase, K. Oka, T. Ito, H. Eisaki, M. Fujisawa, S. Okubo, and H. Ohta: J. Phys. Soc. Jpn. **80** (2011) 083705.
- [12] H. Kuroe, T. Hamasaki, T. Sekine, M. Hase, K. Oka, T. Ito, H. Eisaki, and M. Matsuda: J. Phys.: Conf. Ser. **200** (2010) 022028.
- [13] H. Kuroe, T. Hamasaki, T. Sekine, M. Hase, K. Oka, T. Ito, H. Eisaki, K. Kaneko, N. Metoki, M. Matsuda, and K. Kakurai: Phys. Rev. B **83** (2011) 184423.
- [14] M. Matsumoto, H. Kuroe, T. Sekine, and M. Hase: J. Phys. Soc. Jpn. **81** (2012) 024711.
- [15] H. Kuroe, K. Aoki, R. Itoh, T. Hosaka, T. Hasegawa, M. Akaki, H. Kuwahara, T. Sekine, M. Hase, K. Oka, T. Ito, and H. Eisaki: J. Kor. Phys. Soc. **63** (2013) 542.
- [16] K. Oka, T. Ito, H. Eisaki, M. Hase, T. Hamasaki, H. Kuroe, and T. Sekine: J. Cryst. Growth **334** (2011) 108.
- [17] T. Matsuzaki, K. Ishida, K. Nagamine, I. Watanabe, G. H. Eaton, W. G. Willams: Nucl. Instr. and Meth. A **465** (2001) 365.
- [18] C. Kittel; *Introduction to Solid State Physics* (John Wiley & Sons, Inc., Hoboken, NJ, 2005) 8th ed., p. 326.